

# Mineralogy, Petrology and Geochemistry of the Basalt Flows at Ash-Shuna Ash-Shamaliyya Area, North West Jordan

Ibrahim Ahmad Ali Bany Yaseen, Alaa Yaser Abidrabbu

Institute of Earth and Environmental Sciences, Al al-Bayt University, Mafraq, Jordan

## Email address:

ibanyyaseen@Yahoo.com (I. A. A. B. Yaseen), alaayaser1987@gmail.com (A. Y. Abidrabbu)

## To cite this article:

Ibrahim Ahmad Ali Bany Yaseen, Alaa Yaser Abidrabbu. Mineralogy, Petrology and Geochemistry of the Basalt Flows at Ash-Shuna Ash-Shamaliyya Area, North West Jordan. *Earth Sciences*. Vol. 5, No. 6, 2016, pp. 82-95. doi: 10.11648/j.earth.20160506.11

**Received:** August 29, 2016; **Accepted:** October 5, 2016; **Published:** November 7, 2016

---

**Abstract:** Twenty-seven basaltic fresh rock samples collected from North West Jordan at Ash-Shuna Ash-Shamaliyya area studied. The Ash-Shuna Ash-Shamaliyya basalt (SHB) introduced within Pliocene to Quaternary (recent) volcanism in North West Jordan, and produced within intraplate continental alkali to calc-alkaline basalt. The mineralogy analyses of the SHB rocks are composed of plagioclase, pyroxene, olivine, opaque minerals (iron oxide), and secondary minerals included iddingsite and calcite. The common textures of the SHB were trachytic, glomeroporphyritic, seriate, intergranular, poikilitic, corona, optitic to subophitic, radiate, cumulate, vesicular and amygdaloidal. The geochemical analysis data of SHB indicated that SHB was derived from a slightly fractionation magma as reflected by high MgO concentration (average 8ppm) and Mg#% (average 46%), and high concentration Ni (average 158ppm) and low silica content (average 48wt%). The Geochemical classification of SHB introduced within basaltic to trachybasalt field and calc-alkaline to alkali basalt. The tectonic setting of SHB explained by using discrimination diagrams, Ti-Zr-Y, Ti-Zr-Sr, MgO-FeO(tot)-Al<sub>2</sub>O<sub>3</sub>, and Nb-Y, the SHB plotted within plate, calc-alkali and continental basalt respectively. The Rayleigh fractionation equation modeled for Sr versus Ba vector diagram indicated the SHB had fractionation less than 10% for clinopyroxene, orthopyroxene, olivine and plagioclase.

**Keywords:** Calc-Alkaline Basalt, Tectonic Setting, Fractionation, Ash-Shuna Ash-Shamaliyya, Jordan

---

## 1. Introduction

The basalt in Jordan occurs as sporadic volcanic centers; (vents) along the eastern side of (Bender, 1974). The basaltic rocks are occupying 18% of Jordan area (El-Hasan and Al-Malabeh, 2008). The basalt is associated with continental rifting and in caption of the Dead Sea boundary, and associated between magmatism and tectonic activities, that have produced melted generation into fissure system (Shaw et al., 2003). The basalt in Jordan investigated by (Barberietal., 1979), and reported similar to alkaline Arabia interpolates volcanic fields, erupted within the main fissure systems. The fissures trend to East-West, along the eastern margin of the Dead Sea Rift, on the large basaltic plateau, fissures trend NW-SE direction (Ibrahim et. al., 2003). The volcanism started probably during the middle to late Miocene and recent (13-8Ma) (Moffat, 1988; Camp and Roobol, 1992; Tarawneh et al., 2000). Based on K-Ar age determination the

volcanic activity of Jordan have divided into three major episodes; Oligocene to early Miocene (26.23-22.17Ma), Middle to late Miocene (13.97-8.94Ma), and Late Miocene to Pleistocene (6.95Ma to < 0.15Ma) (Barbarietal., 1979; Moffat, 1988; Duffield et al., 1987; Ilanietal., 2001).

The basalt flows mainly distributed in Jordan from the northeast (NE-basalt plateau) to the north and from the middle parts to the east of the Dead Sea. In general, the extent of the volcanic province is parallel with the NW-SE trending to Wadi Sirhan fault zone that probably caused by tensional forces parallel to the Red Sea. The above mentioned basalt flows were considered by Ibrahim, (1993) as the Harrat Ash-Shaam Basaltic Super-Group, and this term was applied in Jordan to all of the Neogene-Quaternary basalts exposed in the North Arabian Volcanic Province (El-Akhal, 2004). According to Bender, (1974) classified the eruptions of basaltic according to their distribution in three groups; 1) Central Jordan Basalt (basalt volcanoes within the

rift) 2) South Jordan Basalt (the eastern margin basalt) 3) Northeast Jordan basalt, Harrat Al-Sham (plateau basalt), and North west basalt (Harrat Irbid) (Al-Malabeh, 2015; Israa et al., 2016, Smadi, 2016).

The volcanism region extends from Syria through Jordan and into Saudi Arabia (Harrat Al-Shaam), which covers 11,400 km<sup>2</sup> in Jordan (Fig. 1) (Guba and Mustafa, 1988). The volcanic field comprises a series of horizontal lava flows, numerous scoria cones, extensional faults and large fissure eruptions from dykes and numerous vents along the basaltic plateau of north east Jordan (Ibrahim et al., 2003).

The volcanic basalts flow broad at central and north west Jordan have been found to occur in eight places, Tafila, Wadi Dana, Jabal Shiihan, El-Lajjoun, Jurf Al-Darawish, Ghor Al-Katar, Wadi Zarqa-Main and Ash-Shuna Ash-Shamaliyya in the form of plateau basalts. Local flows (wadi fills), or individual volcanic bodies (cones, plugs, and dikes) (Camp and Roobol, 1989; Steinitz and Baratov, 1992). The North West Jordan basalt flow covers the study area of Ash-Shuna Ash-Shamaliyya (Figure 1). The flows constitute the southern part of the Zamlat Bkhila plateau of Syria (Ponikarov et al., 1967) which called as Move Hama plateau (Mor and Steinitz, 1985). The original plateau was deeply dissected and led to the formation of the Yarmouk River (Wiesemann and Abdullatif, 1963). According to Al-Malabeh, 2015, suggested that the Ash Shuna Ash Shamaliyya basalt (SHB) flows including within Umm Quis basalt and have extending to the Harrat Irbid basalt. The main objectives of the study evaluate the geological properties of Ash Shuna Ash Shamaliyya basalt (SHB), and to investigate the mineralogy, petrology, geochemistry and petrogenesis of the basalt flow.

## 2. Geological Setting

Ash-Shuna Ash-Shamaliyya basaltic (SHB) area greatly affected by the uplift and vertical movements of the Jordanian block, as a part of the regional uplift of the Afro-Arabian dome started with the second-stage of the Red Sea spreading over the past 5Ma during late Neogene and Pleistocene to Pliocene times. Huge amounts of Quaternary basalt lavas were erupted from vertical fissures and local vents along regional extensional fault lines (Ghent et al., 1980; Gregory et al., 1982; Coleman et al., 1983; Camp and Roobol, 1989).

The sedimentary rocks formations at the study area are described in detailed (1:50,000) geological map prepared by Basem K., (2000). The geological Formations tertiary to late cretaceous is included; Belqa Group unconformable over lies the Ajlun Group and comprises six formations. These formations are, Wadi Umm Ghudran Formation, exposure and restricted to the south eastern part of the study area. Amman Silicified Limestone Formation, outcrop of this formation is present in the southwestern quarter of the study area mainly within deep wadis. Al Hisa Phosphorite Formation, crops out as discontinuous thin strips along Wadi Ushushal Ghurab, Wadi al Haddad and Wadi al Arab.

Muwaqqar Chalk Marl Formation exposed in Wadi Shallala, Yarmouk River and Warren Wadis. The formation comprise massive, soft white chalk marl cliffs, with Pecten-like bivalves, fish teeth, and vertebrate remain sand occasional tube like horizontal to inclined burrows. Above this, a sequence of alternating soft Chalk and Chalky Limestone at upper part and hard limestone concretion with in clayey marl towards it stop. Umm Rijam Chert-Limestone formation dominates in the northern and western part of Waqqas sheet. This formation divided into three units, lower middle and upper. Massive bedding dominated; thin bedding is common towards the top of the unit. The association of chalk limestone and chert lithologies indicates a quiet open marine bottom condition in shallow to moderate pelagic environment. The presences of oil shale indicate short periods of reducing condition. Shallah chalk Formation, exposed in the north, along wadi Shallala and Nahr al Yarmouk.

The volcanism is an essential feature in the study area gave rise to basalt and tuff, with the exception of Miocene interruptions. Basalt in the study area can be sub divided into the following main types; Plateau basalt, the volcanic, which build the plateau basalt range in age from the Pliocene to the lower Pleistocene from about 5.1-3.5 Ma (Basem K., 2000). Yarmouk basalt, only a few terraces of this basalt remain, approximately 100-200m above the present river bed, age assigned to 0.7Ma. Raqqad basalt, below 100 m level, to the level of the present river bed. It is age ranging from 0.4 to 0.1Ma (Ibrahim, 1993) named these basalts "the Harrat Ash Sham Basaltic Group", covering an area of about 11,400 km<sup>2</sup>; it is an assigned age range from Miocene to Pleistocene (Al-Malabeh, 2003). The north Jordan basalt (Harrat Irbid) for Pliocene to Quaternary adds to 300 km<sup>2</sup> for area cover in North Jordan (Al-Malabeh, 2015; Isra et al., 2016).

The structure of the study area bounded to the west of the Jordan valley, a segment of the major rift structure recognizable from East Africa to South Turkey where a sinistral movement took place during last 27Ma. The study area affected by sharing, compression, and extension and regional dips area few degrees toward the north, northeast and northwest. High westerly dip sac accompanying the North-South step faulting associated with the rift formation well expressed in the western parts of the study area especially the Miocene Waqqas conglomerate Group (Basem K., 2000). Structurally the study area can be subdivided in three main zones, 1) North-South trending zone adjacent to the rift, dominated by NNW to N-S fault; 2) intensely faulted and gently folded southern parts including the extension of Ajlun Structure; 3) fault relatively stable northern and northeastern parts, including Irbid plain and Yarmouk River and fold dominated northwest.

## 3. Sampling and Analytical Techniques

A twenty- seven representative's fresh rock chip samples were collected from the out croup of the ash Ash-Shuna Ash-Shamaliyya area. The samples crushed and powdered using a

stainless steel Jaw Crusher and an Agate Ball Mill machine, to obtain grain size less than  $-60\mu$ . The samples were quartered in order to get a statistically representative (splitter) fraction and powdered using two geochemical techniques at Al al-Bayt University for Water Environment and Arid Regions Research Center. The major elements analyzed on fused glass discs-like pellet (bead) by using a Phillips X-Ray Fluorescence Spectrometry (XRF) Majex PW-2424 Model at the Water Environment and Arid Regions Research Center, Al al-Bayt University. A total of 2gm of the powder samples mixed with 8gm of lithium tetraborate and fused in platinum crucibles over gas burners ( $1000^{\circ}\text{C}$ ) for 1h. The melts poured into a mold to create glass disks. The Loss on Ignition (LOI) determined by the weight lost after melting at  $1000^{\circ}\text{C}$ . The trace elements of Br, Co, Pb and Ni analysed by using

Atomic Absorption Spectrometry (AAS), using by 0.2gm digestion of the samples for Aquaregia solution ( $2.5\text{mlHCl}+2.5\text{mlHNO}_3+5\text{mlHF}$ ) and added 50ml of  $\text{H}_3\text{BO}_3$  at the Al al-Bayt University, Water Environment and Arid Regions Research Center. The elements Sr, Y, Nb and Zr analysed by using Ione Conductive Coupled Plasma Emission Spectroscopy (ICP-AES) at Natural Resources Authority Labs. Thin section prepared at the Al al-Bayt University and Hashemite University and examined under polarizer microscope. The photomicrographs of the samples obtained by using LEICA-DMEP Canon camera in the petrography unit at Natural Resources Authority. The geochemical data processed and pictorially represented by using the computer program Iqpet 32. CIPW-Norm calculations by using the Excel sheet (Hollocher K., 2004).

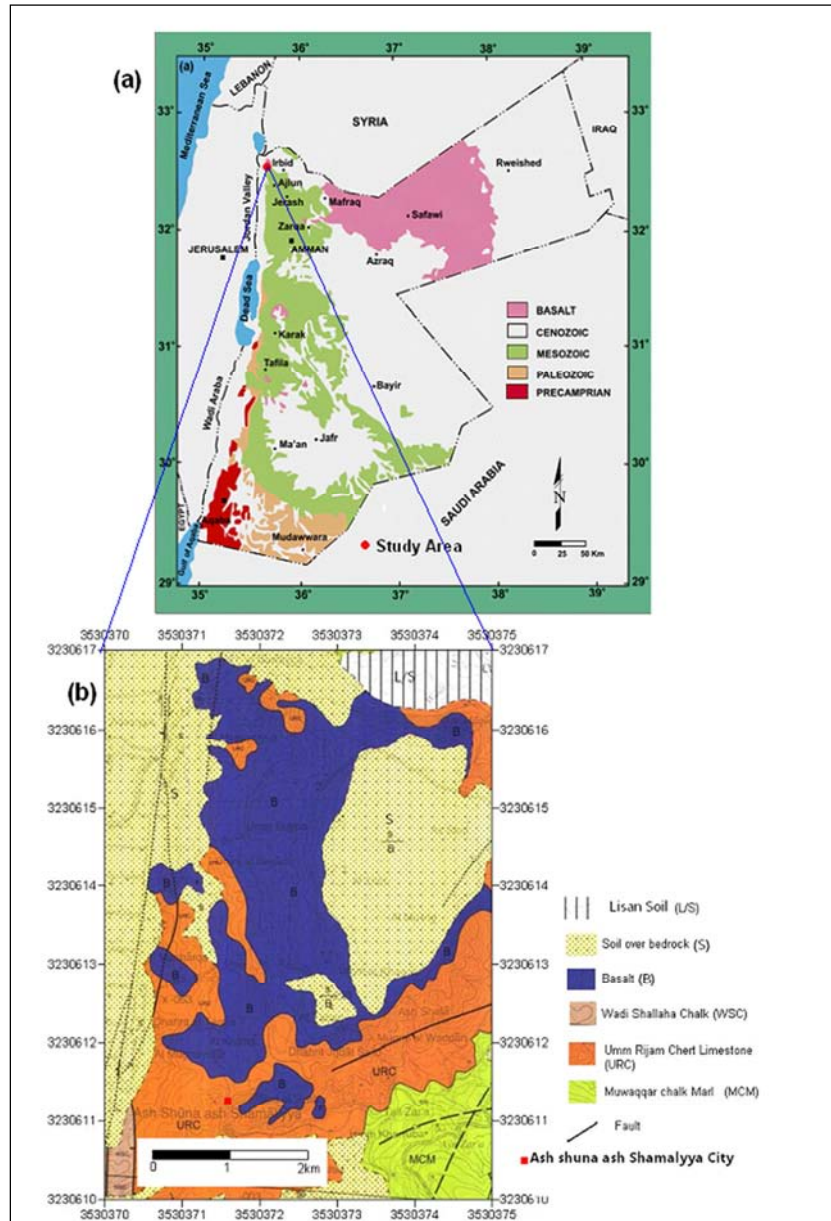


**Fig. 1.** (a):General geological map of Jordan showing the basalt rocks distribution and location of the study area,(b):Geological map of the study area (after Basem K.,2000).

## 4. Mineralogy and Petrology

The SHB samples were melanocratic, holocrystalline, hypidiomorphic fine to medium grained and aphenitic to porphyritic texture. The mineral composition, plagioclase, pyroxene, olivine and opaque minerals (iron oxide). The secondary minerals included iddingsite, calcite and clay minerals. The common textures of the SHB were trachytic, glomeroporphyritic, seriate, intergranular, poikilitic, corona, ophitic to subophitic, radiate, cumulate, vesicular and amygdaloidal.

### 4.1. Plagioclase

Plagioclase is the most abundant minerals in the SHB, it occurs as lath shape, phenocryst crystals, range from medium to coarse grain. It had many unique properties its subhedral to euhedral with tabular shape from 0.5 to 5 mm in length, forming about 45% - 60% vol% of the rock. The crystals show simple and multiple twinning (Fig. 2, 1). The extinction angles on several plagioclase phenocrysts range from 26° to 28°, indicating a labradorite composition (An<sub>50</sub>-An<sub>70</sub>%), which was determined by using the method described by (Kerr, P., 1977). The plagioclase elongated crystals exhibited orientation similar to those of olivine and pyroxene crystals, presenting a trachytic texture (Fig. 2, 2). The glomerophyritic texture (plagioclase, pyroxene, and olivine enclosed in ground mass was noted in clusters of four crystals (Fig. 2, 3). Glomerocrysts are an important consideration in crystal fractionation by crystal settling formation of glomerocrysts may in part explain the settling of plagioclase crystals are less dense than the surrounding of magma. The other hand cumulate texture are shows in interstitial growth of a mineral between earlier ones which are all in contact and give the distinct impression that they accumulated at the bottom of a magma chamber (Fig. 2, 4). Ophitic and Subophitic texture formed for a larger plagioclase crystal completely or partially enclosed by pyroxene or olivine crystals as shown in (Fig. 2, 5 and 6). The Radiate texture are shows in (Fig. 2, 7), which plagioclase elongate crystals diverge from a common nucleus, and may have fan, plume spray or radial shape (Mackenzie et al., 1982). Seriate texture where plagioclase crystals are range from small to large in size, it is formed when the mineral crystals size continuous from the smallest (0.01mm) to the largest (up to 3mm). The Seriate rising due to grain boundary migration during grain course (Fig. 2, 8).

### 4.2. Pyroxene

Pyroxene occurred as colorless at (PPL), and second to third order in interference color (XPL) with anhedral to subhedral crystals, comprising about 12 vol% to 18 vol%. The crystals had assize between 0.25 to 45mm, with perfect parallel cleavage (110), which intersected at 90° in the cross-section (Fig. 2, 9). The pyroxene crystals had an inclined extinction between 46° and 53°, indicating the presence of clinopyroxene of diopside. The clinopyroxene intersected with plagioclase crystals to form ophitic to sub ophitic

texture (Fig. 2, 5 and 6).

### 4.3. Olivine

The olivine phenocrysts are occurred subhedral to anhedral crystals, ranging between 2.5 mm to 5 mm in diameter in the groundmass and forming 14 vol% to 18vol% for modal. The olivine crystals were colorless in (XPL) and second to third order (XPL). Subhedral olivine phenocryst shad high relief, cracks and fracture it lights gray to colorless crystals, parallel extension and had orthorhombic system. Olivine crystals displaying seriate texture (Fig. 2, 8), with high degree of alteration to iddingsite had brownish to red color. The aggregate crystals exhibit glomeroporphyritic texture. Glomeroporphyritic texture where plagioclase and olivine crystals has bunched in aggregate (Fig. 2, 3). Iddingtization was common particularly the edge (rim) produced to form corona texture (Fig. 2, 10), and fracture of the crystals, and some crystals were partially to completely pseudomorphosed to brown iddingsite (Abderahma and El-Akhal, 2004) (Fig. 2, 11and12). The alteration produced as a result from relatively low temperature deuteric alteration process (El-Hasan .and Al- Malabeh., 2008), and the embayment of olivine crystals, because of interaction between melt and olivine crystals during the crystallization process (Cox, K., and Pankhurst R., 1979).

### 4.4. Opaque Minerals

Opaque minerals were commonly found in SHB, forming model about 4 vol% to 8 vol% of the rocks and ranging from 0.2 to 3 mm in size. They mostly occurred as iron oxide phenocrysts scattered throughout the rock and as inclusion within olivine or pyroxene crystals produced poikilitic texture, where olivine crystals completely encloses numerous grains of opaque minerals (Fig. 2, 13). The optical properties of iron oxide were black color with PPL and XPL optics. The norm calculation the oxide mineral represented by 12 wt% norm of ilmenite (FeTiO<sub>3</sub>), hematite (Fe<sub>2</sub>O<sub>3</sub>) and Pervoskite (CaTiO<sub>3</sub>) (Table 1).

### 4.5. Vesicles

The SHB showed irregular elongated or rounded holes (vesicles) size from 3mm to10mm. The long axis was about 3mm to 5 mm width. The vesicles were filled with secondary minerals such as calcite and clay minerals (Fig. 2, 14), and formed about 3 vol%-7 vol% of the rock.

### 4.6. Groundmass

The groundmass of SHB consisted of plagioclase (labradorite), olivine, pyroxene (augite), and opaque minerals (mainly iron oxide), with secondary minerals such as iddingsite, calcite, and chlorite.



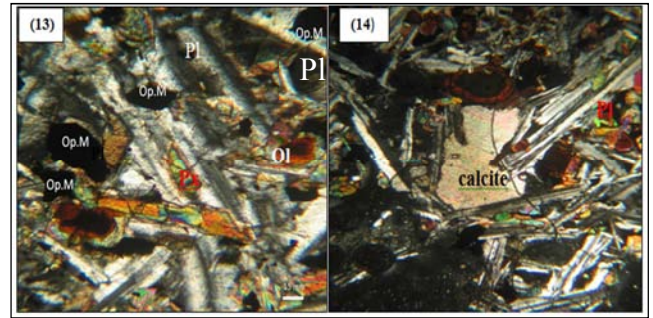
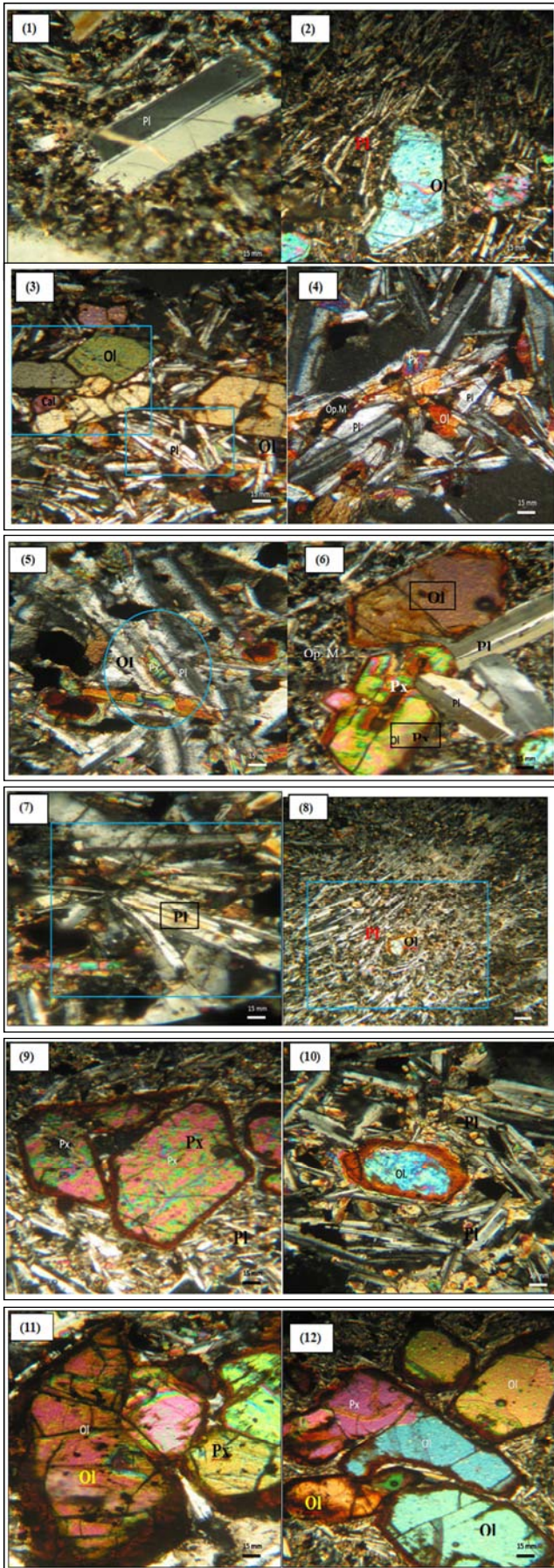


**Fig. 2.** Photomicrograph showing: (1): Simple twinning of plagioclase (XPL, Mag. 10x Sample No. SHB8). (2): Trachytic texture, plagioclase crystals are arranged (XPL, Mag. 4x, Sample No. SHB15). (3): Glomeroporphyritic texture where plagioclase and olivine crystals are bunched in aggregate (XPL, Mag. 4x, Sample No. SHB11). (4): Cumulate texture, plagioclase twinning, and altered olivine (XPL, Mag. 10x, Sample No. SHB24). (5): Ophitic texture where pyroxene crystal wholly enclosed in plagioclase crystal (XPL, Mag. 10x, Sample No. SHB19). (6): Subophitic texture and olivine alteration to iddingsite (XPL, Mag. 10x, Sample No. SHB3). (7): Radiate texture, where plagioclase and olivine crystals in fan shape (XPL, Mag. 10x, Sample No. SHB1). (8): Seriate texture where plagioclase crystals are range from small to large (XPL, Mag. 4x, Sample No. SHB6). (9): perfect two sets of cleavages of pyroxene crystal (XPL, Mag. 10x, Sample No. SHB22). (10): Corona texture, brownish iddingsite surrounding anhedral blue olivine crystal (XPL, Mag. 10x, Sample No. SHB3). (11): Fractured olivine crystals, (XPL, Mag. 10x, Sample No. SHB21). (12 & 13): Poikilitic texture, where pyroxene and olivine crystals completely encloses numerous grains of opaque minerals (iron oxide), (XPL, Mag. 10x, Sample No. SHB8). (14): Vesicular texture, where the vesicles are filled with calcite mineral (XPL, Mag. 10x, Sample No. SHB23). Where: (Ol: olivine, Pl: plagioclase, Px: Pyroxene, Cal: Calcite, Op.M: Opaque minerals, (Magnification 4x=0.1mm, 10x=0.25mm).

## 5. Geochemistry

### 5.1. Major Oxides

The results of chemical analysis of major and trace element of SHB volcanic rocks listed in (Table 1). The sum of major elements ranged from 99.69% to 101.01%, which were within the limit of analytical methods. The SHB rocks exhibit an arrow range of silica ( $\text{SiO}_2$ ) saturation between (44.87 to 50.23 wt%) with an average of (48.02 wt%), which is within the alkaline to subalkaline basalt (Fig. 3a), and it can be classified as basalt using the Total Alkalis-Silica classifications scheme (Fig. 3b). The  $\text{Al}_2\text{O}_3$  contents in the SHB samples range from 13.53 to 14.85 wt%, mean while CaO varies between 9.12 and 11.38 wt%. The binary plot of  $\text{SiO}_2$  versus  $\text{Al}_2\text{O}_3$  and CaO exhibits the inverse relationships between both oxides and  $\text{SiO}_2$  (Fig. 4).

The MgO content of the SHB ranged from 7.13 to 9.84 wt% with an average of 8.10 wt%. The Mg number (Mg#), defined as the molecular proportion of  $[100 * (\text{Mg}^{+2} / (\text{Mg}^{+2} + \text{Fe}^{+2}))]$  (Janner, et al., 1987; Downes, et al., 1995). It is usually used as a petrogenetic indicator for magma fractionation and its primitive volcanic rocks (George, et al., 2010). The Mg# of the SHB range (39.7 to 57.85) with an average of 46.03. The Mg# of the SHB indicates evolved to moderately basalt. As shown in (Fig. 5), Mg# decreases with increasing  $\text{SiO}_2$ . This general trend suggests that fractional crystallization probably plays a role

in decreasing Mg# as a function of increasing SiO<sub>2</sub> (Shaw, J., 2003). The Mg# calculation considers the Fe content in the rocks. According to Wilson, (1989) the value of Mg#>70 considered as a threshold that characterizes primitive magma. Clague, and Ferry, (1982) suggested that a Mg# of 65 is a distinct value. The Fe content of the SHB ranges (7.49 wt% to 12.53 wt%) with an average of 9.86 wt%, indicating that the rocks were enriched in Fe. Shaw, et al., (2003) reported that SiO<sub>2</sub> under saturated magma had a high FeO content of >11 wt% and high MgO content of >7. According to George, et al., (2010) and Moghazi, (2003), it has reported that rocks high Mg# (>60) exhibit lowest content of Nb and Zr and higher content of Ni. The present studies explained to indicate that the basaltic rocks undergo smaller degree of partial melting at high pressures (Bany Yaseen, I., 2014).

The SHB had an average Na<sub>2</sub>O and K<sub>2</sub>O content of 2.24 and 1.73 wt%, respectively. The total Na<sub>2</sub>O+K<sub>2</sub>O values were similar in all the samples, exhibiting an average value of 4.0 wt%. The average ratio of Na<sub>2</sub>O/K<sub>2</sub>O was 1.38, indicating the potassic affinity of the rocks (Fig. 6), and that of Al<sub>2</sub>O<sub>3</sub>/TiO<sub>2</sub> was 4.64, which suggested the basic affinity of the rock.

## 5.2. Trace Elements

The SHB sample found to have a high content of Ni and Co (Table 1). The Ni contents range between 76.5 to 255.5 ppm, with an average value 158 ppm. The Co content ranges between 20.5 to 83.5 ppm with average 57.28 ppm; it documented that SHB fractionation by presence of olivine and clinopyroxene (Winter, 2001). The high content of Ni indicated that the parental magma have been derived through partial melting of peridotite mantle source (Shaw et. al., 2003 and Wilson, 1989). The binary diagram shows the Mg# versus with Ni and Co concentration. The trend of Ni increase with increasing Mg# (Fig. 7a), this result documented with Mudawwara-Quwayra Basaltic Dike (Alnawafleh et. al., 2015). However, the Co decreasing with increasing Mg# (Fig. 7b). This result is the most probably of dilution of Co as are resulted from crustal mixing and assimilation of magma with the country rocks (Wilson, 1989).

The Sr and Zr in the SHB were relatively high contents, Sr ranging between 480 to 844 ppm with average 632 ppm, and Zr for 156 to 620 ppm with average 304 ppm (Table 1). The

Rear Earth Elements (REE) includes Nb and Y content range between 21 to 34 ppm, with average 28 ppm, and 18 to 32 ppm with average 25 ppm respectively. The average Zr/Nb ratio 11.24, Zr/Y ratio 12.36 and Y/Nb ratio 0.94. These ratio documented by Pearce, et. al., (1984) reported for the intercontinental alkali basalt.

## 5.3. Petrogenesis

The chemical analysis of the SHB rock samples for major and trace elements used to construct discriminatory diagrams, for the classification nomenclature, and interpretation of the Petrogenesis of the SHB flows. The classification for Le Maitre et. al., (1989), the SHB samples plotted within alkaline to sub alkaline rock field (Fig. 3a). The AFM diagram shows the SHB samples plotted in the calcalkaline series (Fig. 8a). The ternary diagram for Ti-Zr-Sr diagram shows the samples of SHB plotted within calcalkaline field (Fig. 8b). The tectonic setting for the SHB explains by using the discrimination diagrams for Ti-Zr-Y, MgO-FeO(tot) – Al<sub>2</sub>O<sub>3</sub> and Nb-Y. The samples plotted within plate field (Fig. 9a), continental basalt field (Fig. 9b) and within plate (Fig. 9c) respectively.

The low content of SiO<sub>2</sub> for SHB samples range between 44.87 to 50.23 wt% and high content of MgO (7.13 to 9.46 wt%) and total FeO (7.49 to 12.53 wt%) indicated the natural fractionation of the SHB. The high Mg#% (average 46) for SHB is similar to that reported for rock affected by fractionation or accumulation of clinopyroxene, orthopyroxene, olivine and plagioclase (Ma, et. al., 2011). The Rayleigh fractionation equation for Rollinson, (1993), are used to modeled the mineral fractionation  $C_1/C_0 = F^{(D-1)}$ , where C<sub>1</sub> is the concentration of a trace element in the residual melt; C<sub>0</sub> is the concentration of a trace element in the original melt; F is the fraction of melt that remains, and D is the bulk partition coefficient. The partition coefficient of Sr and Ba modeled of the mineral fractionation vector diagram in (Fig. 10), which indicated that the SHB rock samples had fractions less than 10% of orthopyroxene, clinopyroxene, and traces of olivine and plagioclase. The variation diagram (Fig. 11) shows positive correlated with MgO and liner trend of fractionation phase, this indicating to removal of CaO and MgO from liquid in the coprecipitation of clinopyroxene and plagioclase (Rollinson, 1993).

**Table 1.** Chemical composition of the samples from SHB. The major oxides are given in wt%, trace elements in ppm and CIPW-wt% Norm.

Sample No.	SHB1	2	3	4	5	6	7	8	9	10	11
SiO <sub>2</sub>	48.45	48.67	50.23	47.87	45.97	48.78	49.53	45.59	46.83	46.37	44.87
TiO <sub>2</sub>	3.13	2.96	3.57	3.74	2.98	2.49	2.78	2.87	2.87	3.93	3.82
Al <sub>2</sub> O <sub>3</sub>	13.55	14.72	13.65	14.69	13.68	13.85	13.66	13.69	14.79	13.56	14.68
Fe <sub>2</sub> O <sub>3</sub>	8.98	8.54	7.49	9.87	10.68	12.53	10.46	11.87	10.89	9.94	10.96
MnO	0.34	0.38	0.87	0.35	0.36	0.65	0.54	0.95	0.25	0.48	0.76
MgO	8.45	8.67	8.24	8.16	7.46	8.25	7.36	9.46	8.58	9.24	8.15
CaO	10.67	9.97	9.25	11.38	9.59	9.28	9.75	9.48	9.59	10.48	9.54
Na <sub>2</sub> O	3.67	2.86	1.89	1.95	2.94	1.92	1.98	1.88	1.95	1.89	1.88
K <sub>2</sub> O	1.54	1.26	1.98	0.86	2.86	0.77	1.69	1.69	1.55	1.52	2.56
P <sub>2</sub> O <sub>5</sub>	0.33	0.35	0.36	0.79	0.73	0.36	0.38	0.39	0.46	0.38	0.37
LOI	0.95	1.63	2.49	0.46	2.77	2.13	1.91	1.96	2.28	2.24	2.42
SUM%	100.06	100.01	100.02	100.12	100.02	101.01	100	99.83	100.04	100.03	100.01
Mg#	58.85	50.37	52.38	45.25	49.27	39.7	44.09	44.31	45.9	45.74	42.64

Sample No.	SHB1	2	3	4	5	6	7	8	9	10	11
Na <sub>2</sub> O/K <sub>2</sub> O	2.38	2.26	0.95	2.26	1.03	2.49	1.17	0.96	1.25	1.24	0.73
Al <sub>2</sub> O <sub>3</sub> /TiO	4.32	4.97	3.82	3.92	5.56	4.91	4.91	4.77	5.15	3.45	3.73
Traceelements(PPM)											
Ba(ppm)	235	546	435.5	410.5	505.5	297.5	379.5	529	442	633	677
Co	50	46	25	53.5	36.5	36	45	39.5	20.5	27	62
Pb	5.5	11.5	31	4	23	29.5	16.5	38	9.5	25.5	5
Ni	153.5	163.5	135	203	153.5	76.5	152	108	149.5	164	143.5
Sr	578	680	726	690	658	760	568	579	763	488	679
Y	25	22	28	26	21	19	18	31	32	29	27
Nb	26	27	23	30	29	32	29	30	25	31	22
Zr	290	285	310	298	250	225	178	156	188	221	186
Zr/Nb	11.15	10.56	13.48	9.93	8.62	7.03	6.14	5.2	7.52	7.13	8.45
Zr/Y	11.6	11.6	12.95	11.07	11.46	11.9	11.84	9.89	5.03	5.88	7.62
Y/Nb	0.96	0.81	1.22	0.87	0.72	0.59	0.62	1.03	1.28	0.94	1.23
TiO <sub>2</sub> /Y	0.13	0.13	0.13	0.14	0.14	0.13	0.15	0.09	0.09	0.14	0.14
CIPW-Normw%											
Quartz	---	---	5.03	3.66	---	7.1	5.63	---	1.23	---	---
Anorthite	16.11	23.98	23.5	28.88	16.15	27.32	23.83	24.44	27.65	24.6	24.64
Albite	30.78	24.63	16.41	16.6	24.58	16.41	17.1	16.24	16.84	16.33	16.33
Orthoclase	9.16	7.56	12	5.1	17.37	4.6	10.16	10.22	9.4	9.16	15.48
Diopside	20	11.90	9.48	8.83	17.83	8.56	12.12	11.58	7.11	11.14	8.79
Olivine	8.40	2.62	---	---	8.57	---	---	1.82	---	0.40	7.23
Hypersthen	--	12.68	16.65	---	---	16.8	13.1	16.1	18.57	---	7.38
Apatite	0.76	0.83	0.86	1.83	1.73	0.84	0.9	0.95	1.1	0.90	0.88
Sphene		6.32	6.53	8.15		4.33	5.37	4.42	6.44	6.44	7.38
Ilmenite	0.72	0.83	1.9	0.81	0.23	1.43	1.21	2.0	0.6	1.10	1.71
Hematite	9.10	8.64	7.68	9.9	10.98	12.64	10.66	12.13	11.14	10.16	11.23
Pervoskite	4.73	---	---	---	4.46	---	---	---	---	---	---

Continued

Sample No.	SHB12	13	14	15	16	17	18	19	20	21	22
SiO <sub>2</sub>	49.56	48.48	48.82	49.38	49.95	49.56	48.94	49.45	45.83	47.82	46.85
TiO <sub>2</sub>	3.53	2.68	2.17	2.79	2.62	2.71	2.77	3.79	3.68	2.76	3.65
Al <sub>2</sub> O <sub>3</sub>	13.53	14.68	14.45	13.65	13.55	13.69	14.56	13.56	14.65	13.65	14.53
Fe <sub>2</sub> O <sub>3</sub>	8.86	8.89	8.93	9.89	9.87	8.87	9.87	8.87	10.85	10.89	9.85
MnO	0.43	0.58	0.47	0.16	0.84	0.79	0.42	0.49	0.99	0.64	0.77
MgO	7.69	8.35	8.94	7.78	7.45	8.13	7.15	8.14	8.13	8.14	7.67
CaO	9.78	9.32	9.93	9.12	9.87	9.23	9.28	9.63	9.37	10.82	9.96
Na <sub>2</sub> O	1.94	2.61	1.94	2.92	1.92	1.91	2.93	1.91	1.95	1.95	1.94
K <sub>2</sub> O	1.57	1.58	1.47	1.52	1.45	2.46	1.59	1.58	1.67	1.67	1.59
P <sub>2</sub> O <sub>5</sub>	0.49	0.33	0.36	0.36	0.38	0.41	0.31	0.49	0.37	0.27	0.38
LOI	2.64	2.5	2.21	2.48	1.85	2.27	2.24	2.18	2.51	1.48	2.63
SUM%	100.02	100	99.69	100.05	99.75	100.03	100.06	100.09	100	100.09	99.82
Mg#	46.47	48.43	50.02	44.03	43.01	47.82	44.06	47.85	42.83	42.77	43.77
Na <sub>2</sub> O/K <sub>2</sub> O	1.23	1.65	1.31	1.92	1.24	0.77	1.84	1.21	1.16	1.16	1.22
Al <sub>2</sub> O <sub>3</sub> /TiO	3.83	5.47	6.65	4.89	5.17	5.05	5.25	3.57	3.98	4.94	3.98
Traceelements(PPM)											
Ba	602	621.5	547	643	405	370	652	376	286	572	467
Co	68.5	67	47	70.5	77	65.5	83.5	58	80.5	60.5	79
Pb	12	14	25.5	9	11	7	13	14	8	12	9
Ni	195.5	128	103	115.5	157.5	123	138.5	129	218.5	234	189
Sr	580	520	612	659	496	584	644	812	758	490	745
Y	30	24	22	26	28	32	23	22	25	22	26
Nb	24	21	23	27	32	30	29	24	23	34	32
Zr	350	290	255	198	390	360	410	620	567	320	450
Zr/Nb	14.58	13.81	11.09	7.33	12.19	12	14.14	25.83	24.65	9.41	14.06
Zr/Y	6.89	11.67	12.08	11.59	7.62	13.93	11.25	17.83	28.18	22.68	14.55
Y/Nb	1.25	1.14	0.96	0.96	0.88	1.07	0.79	0.92	1.09	0.65	0.81
TiO <sub>2</sub> /Y	0.12	0.11	0.1	0.11	0.09	0.08	0.12	0.17	0.15	0.13	0.14
CIPW-normw%											
Quartz	5.6	0.06	2.71	1.4	6.92	2.85	0.75	5.35	0.23	1.25	2.08
Anorthite	24.21	24.27	27	20.14	24.6	24.97	25.38	16.5	26.66	23.59	26.94

Sample No.	SHB12	13	14	15	16	17	18	19	20	21	22
Albite	16.84	22.67	16.84	25.5	16.58	16.5	9.63	9.51	16.92	16.75	16.92
Orthoclase	9.51	9.57	8.92	9.22	8.74	14.95	9.63	8.0	10.63	10.52	9.75
Diopside	9.16	10.92	12.17	11.67	13.5	12.55	11.68		7.72	17.40	9.24
Hypersthen	15.41	16.25	17.2	14.41	12.7	12.8	12.86	16.97	7.17	17.12	15.36
Apatite	0.78	0.78	0.85	0.85	0.90	0.97	0.70	1.15	0.88	0.68	0.9
Sphene	5.06	5.06	4.12	6.54	4.15	4.51	5.71	6.1	6.38	4.99	7.0
Ilmenite	1.3	1.3	1.10	0.36	1.88	1.77	0.96	1.11	2.22	1.45	1.73
Hematite	9.12	9.12	9.16	10.14	10.10	9.10	10.10	9.1	11.12	11.03	10.13

Continued

Sample No.	SHB23	24	25	26	27	Min.	Max.	average
SiO <sub>2</sub>	47.53	46.86	45.97	49.57	48.73	44.9	50.23	48.02
TiO <sub>2</sub>	3.73	2.86	3.68	2.69	2.68	2.17	3.93	3.11
Al <sub>2</sub> O <sub>3</sub>	13.59	14.85	13.87	14.66	13.86	13.5	14.85	14.07
Fe <sub>2</sub> O <sub>3</sub>	9.85	8.84	10.96	9.85	8.98	7.49	12.53	9.86
MnO	0.54	0.85	0.85	0.43	0.79	0.16	0.99	0.59
MgO	7.13	8.13	7.35	8.13	8.12	7.13	9.46	8.09
CaO	9.85	10.78	10.81	9.48	9.37	9.12	11.38	9.84
Na <sub>2</sub> O	2.92	1.89	1.95	1.98	2.99	1.88	3.67	2.24
K <sub>2</sub> O	2.69	1.86	1.58	1.76	2.35	0.77	2.86	1.73
P <sub>2</sub> O <sub>5</sub>	0.33	0.39	0.36	0.37	0.32	0.27	0.79	0.40
LOI	1.86	2.76	2.63	1.16	1.86	0.46	2.77	2.09
SUM%	100.02	100.07	100.01	100.08	100.05	99.7	101.01	100.04
Mg#	41.99	49.66	39.86	45.21	47.48	39.7	58.85	46.07
Na <sub>2</sub> O/K <sub>2</sub> O	1.08	1.02	1.23	1.12	1.27	0.73	2.49	1.38
Al <sub>2</sub> O <sub>3</sub> /TiO	3.64	5.19	3.76	5.44	5.17	3.45	6.65	4.64
Traceelements(PPM)								
Ba	621	404	534	532	268	235	677	481.15
Co	72	66.5	64.5	70.5	75	20.5	83.5	57.28
pb	6	10	5	9	7	4	38	13.72
Ni	109.5	154.5	179	234.5	255.5	76.5	255.5	158.02
Sr	734	844	634	532	676	488	844	647.74
Y	24	23	26	27	29	18	32	25.44
Nb	26	31	28	34	27	21	34	27.74
Zr	321	234	341	287	233	156	620	304.19
Zr/Nb	12.35	7.55	12.18	8.44	8.63	5.2	25.83	11.24
Zr/Y	17.31	13.38	10.17	13.12	10.63	5.03	28.18	12.36
Y/Nb	0.92	0.74	0.93	0.79	1.07	0.59	1.28	0.93
TiO <sub>2</sub> /Y	0.16	0.12	0.14	0.1	0.09	0.08	0.17	0.12
CIPW-normw%								
Quartz	---	---	1.16	3.87	---	0.06	7.1	3.16
Anorthite	16.11	27.30	25.10	26.2	17.77	16.11	28.88	23.62
Albite	25.13	16.41	16.92	16.92	25.81	9.51	30.78	18.45
Orthoclase	16.20	11.28	9.57	10.52	14.12	4.6	17.37	10.42
Diopside	16.11	14.37	14.35	9.10	16.30	7.4	20	12.1
Olivine	7.44	0.53	---	---	7.75	0.4	8.57	4.97
Hypersthen	---	13.23	12.15	16.25	1.75	1.75	18.57	13.69
Apatite	0.78	0.92	0.86	0.85	0.76	0.76	1.83	0.94
Sphene	4.70	4.75	6.81	5.41	4.4	4.12	8.15	5.65
Ilmenite	1.20	1.90	1.90	0.98	1.77	0.23	2.22	1.31
Hematite	10.0	9.08	11.25	9.96	9.15	7.68	12.64	10



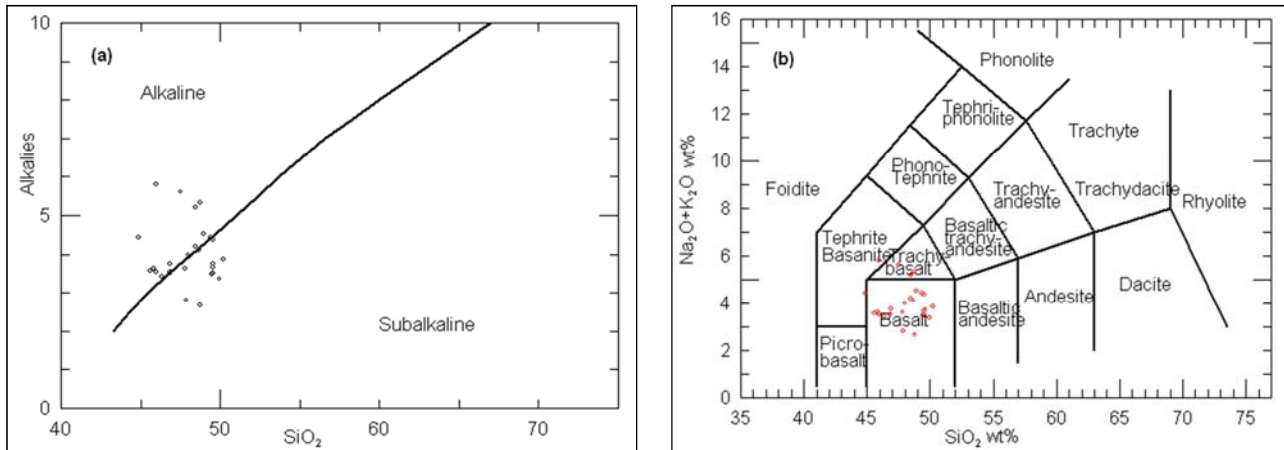


Fig. 3. Chemical classification SHB using (a) TAS vs. SiO<sub>2</sub> (b): Total alkali vs. SiO<sub>2</sub> (Le Maitre et al., 1989).

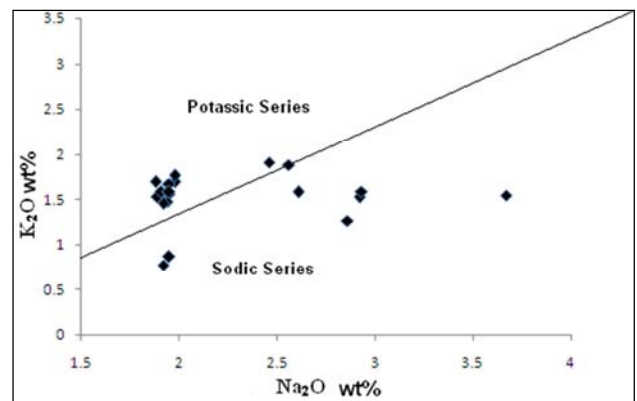
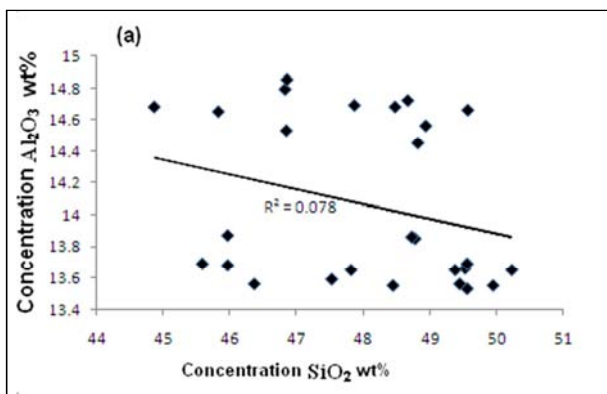


Fig. 6. Na<sub>2</sub>O versus K<sub>2</sub>O of the SHB samples (Middelmost, 1975).

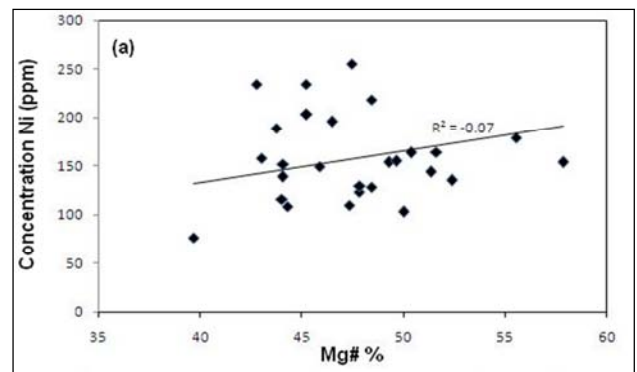
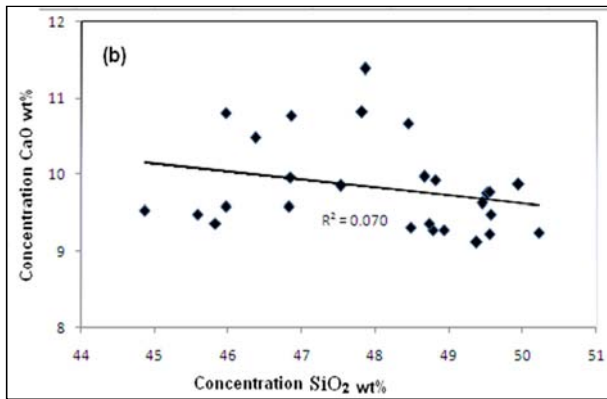


Fig. 4. (a) SiO<sub>2</sub> vs. Al<sub>2</sub>O<sub>3</sub>, and (b) SiO<sub>2</sub> vs. CaO data.

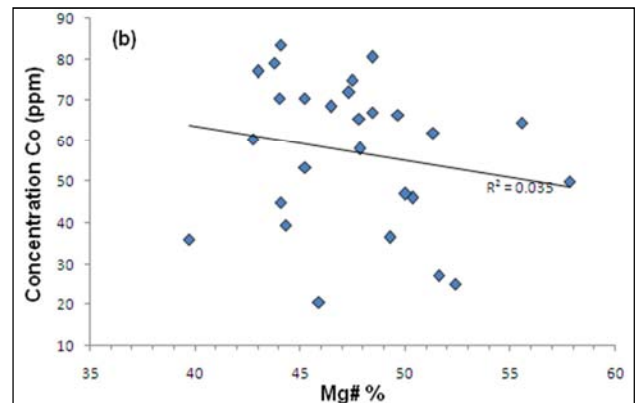
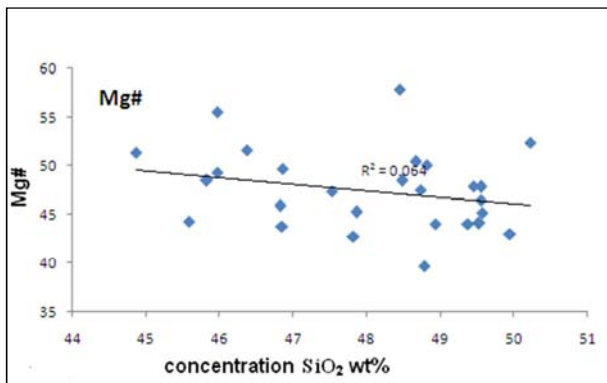


Fig. 5. SiO<sub>2</sub> versus Mg# data.

Fig. 7. (a) Mg# versus Ni, (b) Mg# versus Co.

The geochemical analysis of the major and trace elements used to explain the natural source of SHB, and it used to explain the mantle sources and partial melting of the basalt. This indicates by using trace element ratios and spider diagram (Peltz, and Bratosia, 1986). The high content of Zr/Y (average 12.36) and  $\text{TiO}_2/\text{Y}$  ratios (average 0.12) and low content of Y (average 25.44) indicate that to the garnet-bearing source rocks (Frey, et. al., 1978 and Jenner, et. al., 1987). The spider diagram for Normal Mid-ocean Ridge Basalt (NMORB) for the studied volcanic rocks (Fig. 12a) presented enrichment of the strongly incompatible (LILE) such as Ba and K, and depletion of Nb and Sr relatively to K, and enrichment of Pb. The heavy rare earth elements (HREE) enriched with Zr and depletion of Nb and Y, which showed high similarity to MORB (Fig. 12b and c). The mafic volcanic SHB exhibited negative Nb anomalies and positive Pb anomalies, but presented higher LILE enrichments. The positive anomalies Ba and negative anomalies of Sr and P may be attributed to the fractionation of feldspar for Ba and Sr, and apatite for P depletion (Moghazi, M., 2003). The primitive mantle value of the rock (Fig. 12c) showed appositve Nb peak, which conforms to the tertiary to recent continental alkali basalt provinces (Sun and Mac Donough, 1989; Norry, and Fitton, 1993; El-Akhal, 2004) and indicates that the SHB is the product of lithosphere from upwelling asthenospheric mantle (Bany Yaseen, I., 2016; Ma, et. al., 2011; El-Hasan, and Al-Malabeh, 2008; Wilson, 1989; Thompson, 1987).

## 6. Discussion

The data analysis of the major and trace elements for the SHB samples used to construct discriminatory plots, which applied for the classification, nomenclature, tectonic setting and petrogenesis of the SHB. Based on the Le Maitre et. al., (1989) classification, the SHB samples, plotted within alkaline to subalkaline rock field (Fig. 3a), and within basalt to trachy basaltic field (Fig. 3b). The AFM diagrams shows the SHB samples plotted within the calcalkaline series (Fig. 8a). The ternary diagram for Ti-Zr-Sr diagram shows the samples of SHB plotted within calcalkaline field (Fig. 8b). The tectonic setting for the SHB explains by using three discrimination diagrams, Ti-Zr-Y, for Pearce and Cann, (1973),  $\text{MgO}-\text{FeO}(\text{tot})-\text{Al}_2\text{O}_3$  for Pearce et. al., (1977) and Nb-Y for Pearce et. al., (1984). The samples plotted within plate field (Fig. 9a), continental basalt field (Fig. 9b) and within plate field (Fig. 9c) respectively.

The low content of  $\text{SiO}_2$  for SHB samples range between 44.87 to 50.23 wt% and high content of MgO (7.13 to 9.46 wt%) and total FeO (7.49 to 12.53 wt%) indicated the natural fractionation of the SHB. The high Mg#% (average 46) for SHB is similar to that reported for rock affected by fractionation or accumulation of clinopyroxene, orthopyroxene, olivine and plagioclase (Ma, et. al., 2011). The variation diagram CaO verses MgO (Fig. 10) shows positive correlated with MgO and liner trend of fractionation phase, this indicating to removal of CaO and MgO from

liquid in the coprecipitation of clinopyroxene and plagioclase (Rollinson, 1993).

The Rayleigh fractionation equation for Rollinson, (1993)  $[C_1/C_0 = F^{(D-1)}]$ , are used to modeled the mineral fractionation for the SHB flows. The partition coefficient of Sr and Ba modeled of the mineral fractionation vector diagram in (Fig. 11), which indicated that the SHB rock samples had fractions less than 10% of orthopyroxene, clinopyroxene, and traces of olivine and plagioclase. The batch melting equation for Rollinson, (1993) used to model the degree of partial melting of the SHB. The equation  $(C_1/C_0 = 1/[D_0 + F]^{(1-D_0)})$ . The distribution coefficient model for Ni and Co, and the concentration of the large ion lithophile elements (LILE) was found to exhibit primitive composition (Peltz and Bratosia, 1986). The degree of partial melting (F) calculated by using the concentrations of the oceanic crusts sources. The studied SHB samples show an average partial melting degree less than 10%, which documented with the previously published results for Jordanian and Arabian interpolate basalt (Shaw et. al., 2003; El-Hasan and Al-Malabeh, 2008; Shaw et. al., 2007; Frey et. al., 1978).

The geochemical analysis of the major and trace elements used to explain the natural sources of SHB, and it used to explain the mantle sources of the basalt. This indicates by using trace element ratios and spider diagram (Peltz and Bratosia, 1986). The high content of Zr/Y (average 12.36) and  $\text{TiO}_2/\text{Y}$  ratios (average 0.12) and low content of Y (average 25.44 ppm) indicate that to the garnet-bearing source rocks (Frey et. al., 1978 and Jenner et al., 1987). The spider diagram for Normal Mid-ocean Ridge Basalt (NMORB) for the studied volcanic rocks (Fig. 12a) presented enrichment of the strongly incompatible (LILE) such as Ba and K, and depletion of Nb and Sr relatively to K, and enrichment of Pb. The heavy rare earth elements (HREE) enriched with Zr and depletion of Nb and Y, which showed high similarity to MORB (Fig. 12b and c). The mafic volcanic SHB exhibited negative Nb anomalies and positive Pb anomalies, but presented higher LILE enrichments. The positive anomalies Ba and negative anomalies of Sr and P may be attributed to the fractionation of feldspar for Ba and Sr, and apatite for P depletion (Moghazi M., 2003). The primitive mantle value of the rock (Fig. 12c) showed appositve Nb peak, which conforms to the tertiary to recent continental alkali basalt provinces (Sun and Mac Donough, 1989; Norry, and Fitton, 1993; El-Akhal, 2004) and indicates that the SHB is the product of lithosphere from upwelling asthenospheric mantle (Bany Yaseen, I., 2016; Ma, et. al., 2011; El-Hasan, and Al-Malabeh, 2008; Wilson, 1989; Thompson, 1987).

## 7. Conclusions

The Pliocene to Quaternary (recent) volcanism in North West Jordan produced within intraplate continental alkali to calc-alkaline basalt. The study area covered Ash-Shuna Ash-Shamaliyya basaltic area. The following is the conclusion of the present study:

1. The mineral composition of SHB is as follows: plagioclase, pyroxene, olivine, and opaque minerals (iron oxide). The secondary minerals included iddingzite, calcite and clay. The common textures of the SHB observed trachytic, glomeroporphyritic, seriate, intergranular, poikilitic, corona, ophitic to subophitic, radiate, cumulate, vesicular and amygdaloidal.
2. The chemical classification of SHB for basalt to trachy basalt, calc- alkaline to alkali basalt and includes into potassic series.
3. The tectonic setting for the discrimination diagram showed that the SHB samples plotted within plate basalt, continental basalt.
4. The vector diagram for fractional crystallization of Sr and Ba model for SHB presence of fractions less than 10% of clinopyroxene, orthopyroxene, olivine and plagioclase. The batch melting of the SHB for distribution of Ni and Co indicated a partial batch melting of SHB less than 10% as documented with publishing for Jordanian and Arabian interpolate.
5. The variation diagram for MgO versus CaO shows positive correlated with MgO and liner trend of fractionation phase, this indicating to removal of CaO and MgO from liquid in the coprecipitation of clinopyroxene and plagioclase.
6. The spider diagram for NMORB, primitive mantle and MORB showed enrichment of the incompatible LILE such as Ba and K, and depletion of Nb and Sr relatively to K and enrichment of Pb. The heavy rare earth elements (HREE) enriched with Zr and depletion of Nb and Y, which similarity to MORB. Furthermore, SHB exhibited negative Nb and positive Pb anomalies, but higher LILE enrichments. The positive anomalies Ba and negative anomalies of Sr and P attributed to the fractionation of feldspar for Ba and Sr, and apatite for P depletion. The primitive mantle value of the rock showed apposite Nb peak, which conforms to the tertiary to recent continental alkali basalt provinces and indicates that the SHB is the product of lithosphere from upwelling gas then asthenospheric mantle.

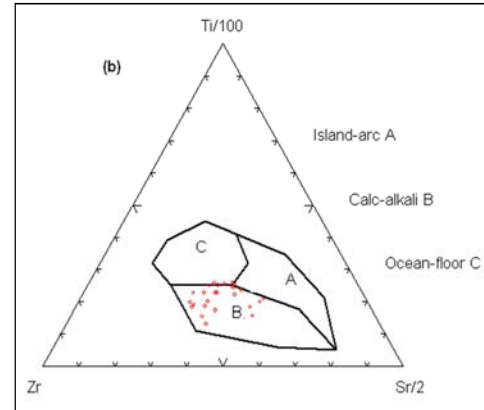
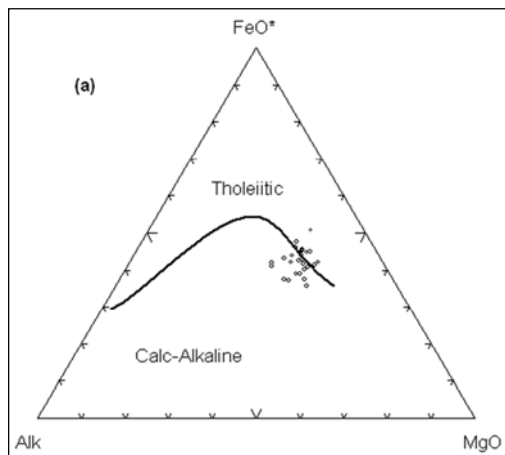


**Fig. 8.** (a) AFM diagram showing the boundary between the calc-alkaline field and tholeiitic field for SHB (Le Maitre et. al., 1989); (b) Ti-Zr-Sr discrimination diagram for SHB (Pearce et. al., 1977).

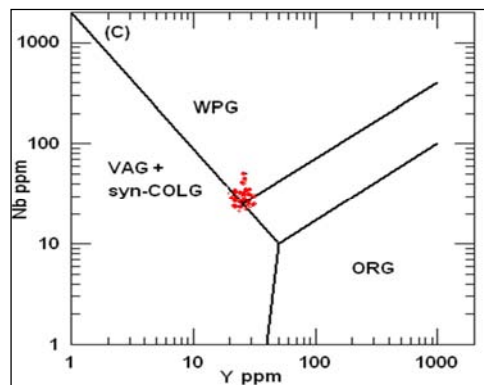
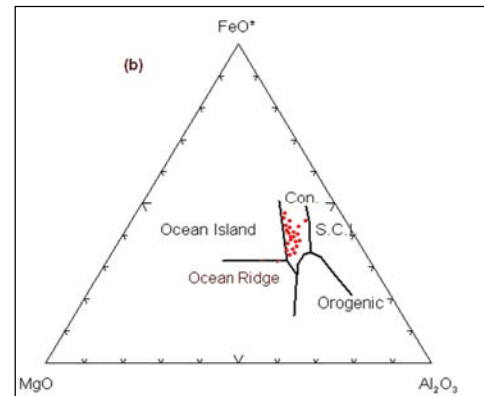
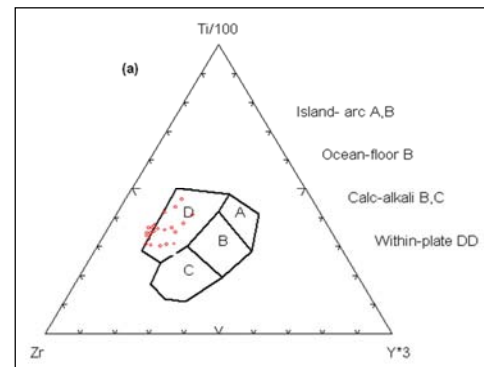


**Fig. 9.** (a) Ti-Zr-Y discrimination diagram for SHB (Pearce ,and Cann, 1973); (b) MgO-FeO(10t)-Al<sub>2</sub>O<sub>3</sub> discrimination diagram for SHB (Pearce et. al., 1977); (c) Nb-Y discrimination diagram for SHB (Pearce et. al., 1984).

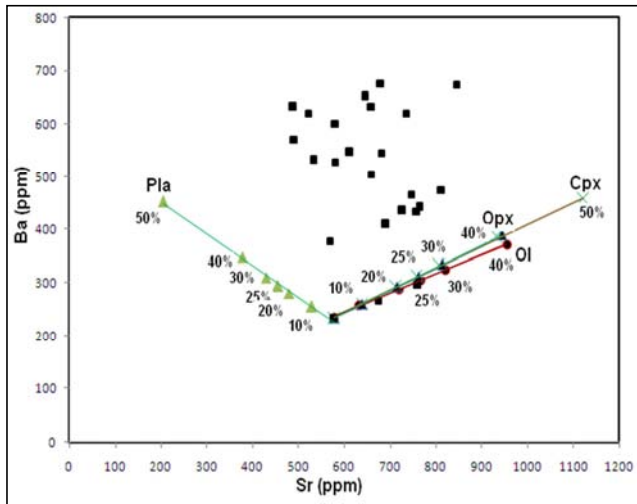


Fig. 10. Sr versus Ba modeled mineral fractionation vector diagram for the SHB rock samples studied. Fractionation trends shown for 10%, 20%, 25%, 30%, 40% and 50% fractional crystallization of minerals: plagioclase (Pla), clinopyroxene (Cpx), orthopyroxene (Opx), and olivine (Ol).

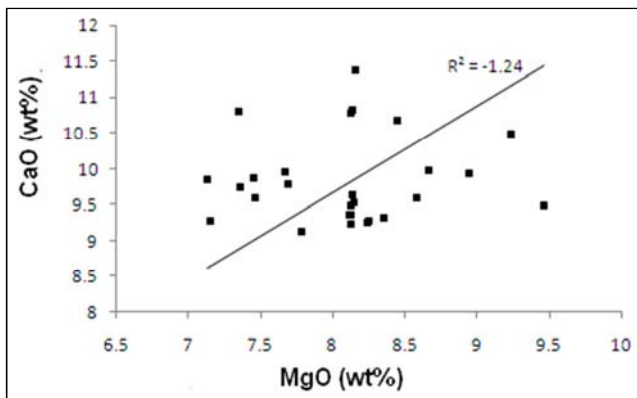


Fig. 11. MgO versus CaO for SHB, shows the fractionation phase.

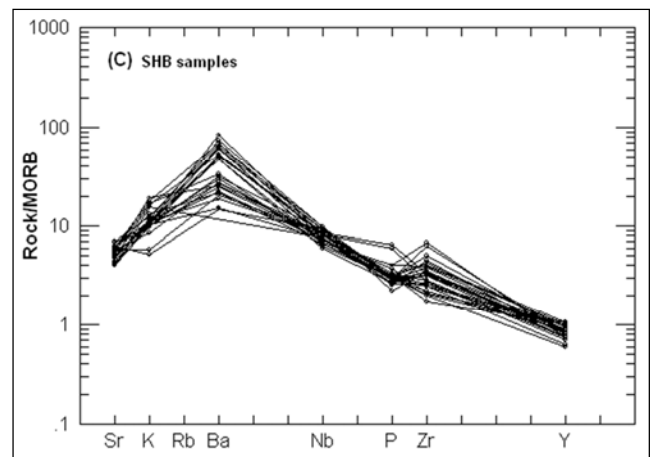
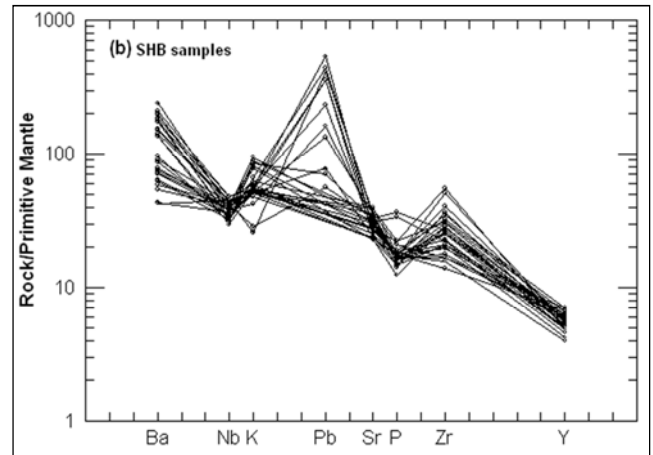
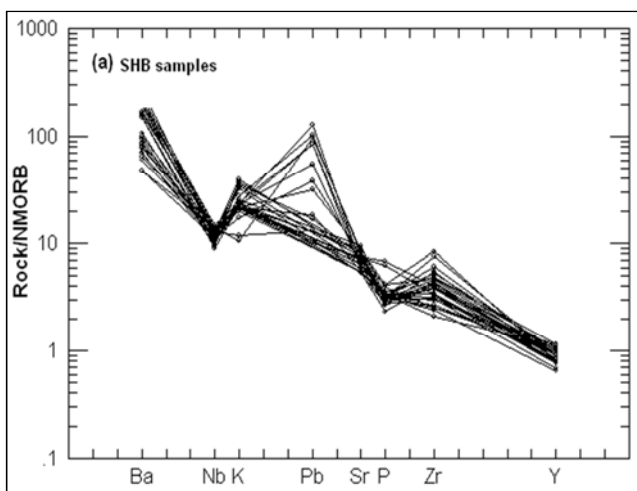


Fig. 12. (a) Spider diagram of incompatibility elements from the SHB. (a) NMORB-Normalized incompatible element plots (Pearce, et. al., 1984); (b) Primitive mantle source elements; (c) Mid Ocean Ridge Basalt (MORB) (Pearce, 1983) show an increasing in compatibility with mantle rocks.

## Acknowledgements

The author is thankful to Al al-Bayt University (Water, Environment and Arid Regions Research Centre), for performing the XRF analysis for major elements and Br, Co, Pb and Ni by using Atomic Absorption Spectrometry. The author grateful to Natural Resources Authority (NRA) lab to help to analysis Sr, Y, Nb and Zr by using Ione Conductive Coupled Plasma Emission Spectroscopy (ICP-AES), and also thanks to geologists Asmaa Al-Qarneh and Muntha Saleem from petrology and petrography unit to help Photomicrographs preparation. The author thanks for Mr. Adnan Mashaqbeh from Al al-Bayt University and Mr. Tareq Al-Bashetti from the Hashemite University for their help in thin sections preparation.

## References

- [1] Abderahman, N. and El- Akhal, H., 2004: Mineralogical composition of Jordan and its physical properties as construction material. ABHATHAL-YARMOUK: "Basic Sci. & Eng., V. 13, pp. 283-300.



- [2] Al- Malabeh, A., 2015: Geological Location map of Basalt flows in north Jordan. Yarmouk University, Department of the Earth and environmental sciences, Irbid Jordan.
- [3] Al-Malabeh, A., 2003: Geochemistry and Volcanology of Jabal Al-Rufiy at, Strombolian Monogenic Volcano, Jordan. *Dirasat*, V. 30, pp. 125-140.
- [4] Alnawafleh, H., Tarawneh, K., Ibrahim, K., Zghoul, K., Titi, A., Rawashdeh, R., Moumani, K. and Masri, A., 2015: Characterization and Origin of the Miocene Mudawwara-Quwayra Basaltic Dike, Southern Jordan. *International Journal of Geosciences*, V. 6, pp. 869-881. <http://dx.doi.org/10.4236/ijg.2015.68071>
- [5] Bany Yaseen I. A. A., 2016: Petrography, Geochemistry and Petrogenesis of Basal Flow from Ar-Rabba Area, Central Jordan, *International Journal of Geosciences*, V.7, pp.378-396, <http://dx.doi.org/10.4236/ijg.2016.73030>
- [6] Bany Yaseen, I. A. A. 2014: Contribution to the Petrography, Geochemistry, and Petrogenesis of Zarqa-Ma'in Pleistocene Alkali Olivine Basalt Flow of Central Jordan, *International Journal of Geosciences*, V.5, pp.657-672. <http://dx.doi.org/10.4236/ijg.2014.56059>
- [7] Barberi, F., Capaldi, G., Gasperini, P., Marinelli, G., Santacrose, R., Scandone, R., Treuil, M. and Varet, J., 1979: Recent Basaltic Volcanism of Jordan and Its Implications on the Geodynamic Evolution of the Afro-Arabian Rift System. *Accademia Nazionale Dei Lincei, Atti Dei Convegni Lincei*, Rome, pp. 667-683.
- [8] Basem K., 2000: Geological Map of Ash-Shuna Ash-Shamaliyya, Natural Resources Authority (NRA), Geology Directorate, Amman, Jordan.
- [9] Bender, F., 1974: Geology of the Arabian Peninsula, Jordan. US Geological Survey Professional Paper, V.36, pp.560-561
- [10] Camp, V. and Roobol, M., 1992: Upwelling Asthenosphere Beneath Western Arabian and Its Regional Implication. *Journal of Geophysical Research*, V. 97, pp.15255-15271. <http://dx.doi.org/10.1029/92JB00943>
- [11] Camp V. E. and M. J. Roobol. (1989): Upwelling Asthenosphere Beneath Western Arabia and Its Regional Implications, *Journal of Geophysical Research*, 255-271. <http://dx.doi.org/10.1029/92JB00943>
- [12] Colemann, R. G., Gregory, R. T., and Brown, G. R., 1983: Cainozoic volcanic rocks of Saudi Arabia. Saudi Arabian Deputy Ministry for Mineral Resources Open-File Report USGS-OF-03093, 82p.
- [13] Clague, D. and Ferry, F., 1982: Petrology and Trace Elements Geochemistry of Honolulu Volcanism: Implication for the Ocean Mantle below Hawaii. *Journal of Petrology*, V. 23, pp. 447-504. <http://dx.doi.org/10.1093/petrology/23.3.447>
- [14] Cox, K., Bell, J. and Pankhurst, R., 1979: *The Interpretation of Igneous Rocks*. Springer, London. <http://dx.doi.org/10.1007/978-94-017-3373-1>
- [15] Downes, H., Seghed, I., Szakacs, A., Dobasi, G., James, D., Vaselli, O., Rigby, I., Ingram, G., Rex, D. and Peckskay, Z., 1995: Petrology and Geochemistry of Late Tertiary-Quaternary Mafic Alkali Volcanism in Romania. *Lithos*, V. 35, pp. 65-81. [http://dx.doi.org/10.1016/0024-4937\(95\)91152-Y](http://dx.doi.org/10.1016/0024-4937(95)91152-Y)
- [16] Duffield, W., Edwin, A., McKee, H., Salem, F. and Teimeh, M., 1987: K-AR ages, Chemical Composition And Geothermal significance of Cenozoic Basalt near the Jordan Rift. Technical report. NRA, Amman.
- [17] El- Akhal, H., 2004: Contribution to the petrography, geochemistry, and tectonic setting of the basalt flows of the Umm-Qais plateau, north Jordan. *Geological Bulletin of Turkey*, V. 47, pp.1-12.
- [18] El-Hasan, T. and Al-Malabeh, A., 2008: Geochemistry, Mineralogy and Petrogenesis of El-Lajoun Pleistocene Alkali Basalt of Central Jordan. *Jordan Journal of Earth and Environmental Sciences*, V. 1, pp. 53-62.
- [19] Frey, F. A., Green, D. H. and Roy, S. D., 1978: Integrated Models of Basalt Petrogenesis: A Study of Quartz Olivine to Olivine Melilites from South Eastern Australia Utilizing Geochemical and Experimental Petrological Data. *Journal of Petrology*, V. 19, pp. 463-513. <http://dx.doi.org/10.1093/petrology/19.3.463>
- [20] George, S., John, M., Costas, X. and Gavin, H., 2010: Petrogenesis of Latest Miocene-Quaternary Continental Intraplate Volcanism along the Northern Dead Sea Fault System (Al-Ghab-Homs Volcanic Field), Western Syria: Evidence for Lithosphere-Asthenosphere Interaction. *Journal of Petrology*, pp. 1-30.
- [21] Ghent, E. D., Coleman, R. G., and Hadley, D. G., 1980: Ultramafic inclusion and host alkali olivine basalts of southern coastal plain of the Red Sea. Saudi Arabia. *Amer. J. Sci*, pp. 280-284, pp. 499-527.
- [22] Gregory, R. T., Coleman R. G., and Brown, G. F., 1982: Cenozoic volcanic rocks of Saudi Arabia. Evidence from continent for two stages of opening of the Red Sea. *Geol. Sci. Am. Prog.*, V. 14(7). pp. 502.
- [23] Guba, I. and Mustafa, H., 1988: Structural Control of Young Basaltic Fissure Eruption in the Plateau Basalt Area of the Arabian Plate, Northeastern Jordan, *Journal of Volcanology and Geothermal Research*, pp. 319-334.
- [24] Hollocher, K., 2004: CIPW Norm Calculation Program. Geology Department, Union College.
- [25] Ibrahim, K. M., Tarawneh, K., Rabbaa, I., 2003: Phases of activity and geochemistry of basaltic dike systems in northeast Jordan parallel to the Red Sea. *J. Asian Earth Sci.* V. 21, pp. 467-472.
- [26] Ibrahim, K. M., 1993: The geological framework for the Harrat Ash Shaam Basaltic Super-Group and its volcanic evolution. NRA, Geological Mapping Division Bulletin 25, pp. 33.
- [27] Ilani, S., Harlavan, Y., Tarawneh, K., Rabba, I., Weinberger, R., Ibrahim, K., Peltz, S. and Steinitz, G., 2001: New K-Ar Ages of Basalts from the Harrat Asham Volcanic Field in Jordan: Implications for the Span and Duration of Upper Mantle Upwelling Beneath the Western Arabian Plate. *Geology*, V. 29, pp. 171-174. [http://dx.doi.org/10.1130/0091-7613\(2001\)029<0171:NKAAOB>2.0.CO;2](http://dx.doi.org/10.1130/0091-7613(2001)029<0171:NKAAOB>2.0.CO;2)
- [28] Israa S. Abu-Mahfouz, Ahmad A. Al-Malabeh and Shaher M. Rababeh, 2016: Geo-engineering evaluation of Harrat Irbid Basaltic Rocks, Irbid District—North Jordan, *Arab J. Geosci.* V. 9: pp. 412-421; DOI 10.1007/s12517-016-2428-4
- [29] Kerr, P., 1977: *Optical Mineralogy*. John Wiley and Sons, New York.
- [30] Jenner, G., Gawood, P., Rautenschlein, M. and White, W., 1987: Composition of Back-Arc Basin Volcanic Valufa Ridge Lau Basin: Evidence for a Slab-Derived Component in Their Mantle Source. *Journal of Volcanology and Geothermal Research*, V. 32, pp. 209-222. [http://dx.doi.org/10.1016/0377-0273\(87\)90045-X](http://dx.doi.org/10.1016/0377-0273(87)90045-X)

- [31] Le Maitre, R. W., Bateman, P., Dudek, A., Keller, J., Lameyre Le Bas, M. J., Sabine, P. A., Schmid, R., Sorensen, H., Streckeisen, A., Woolley, A. R. and Zanettin, B., 1989: A Classification of Igneous Rocks and Glossary of Terms. Black well, Oxford.
- [32] Mackenzie, W. S., Donaldson, C. H., Guilford, C., 1982: Atlas of igneous rock and their textures. England: Longman Scientific and Technical.
- [33] Ma, G. S.-K., Malpas, J., Xenophontos, C. and Chan, G. H.-N., 2011: Petrogenesis of Latest Miocene-Quaternary Continental Intraplate Volcanism along the Northern Dead Sea Fault System (Al-Ghab-Homs Volcanic Field), Western Syria: Evidence for Lithosphere-Asthenosphere Interaction. *Journal of Petrology*, pp. 1-30.
- [34] Middelmost, E., 1975: The Basalt Clan. *Earth-Science Reviews*, V.11, pp.337-564. [http://dx.doi.org/10.1016/0012-8252\(75\)90039-2](http://dx.doi.org/10.1016/0012-8252(75)90039-2)
- [35] Moffat D. T., 1988: A Volcaotectonic Analysis of the Cenozoic Continental Basalts of Northern Jordan; Implications for Hydrocarbon Prospecting in the Block.B Area. Unpubl. Report. University college of Swansen, Uk.
- [36] Moghazi, A. M., 2003: Geochemistry and Petrogenesis of a High-K Calc-Alkaline Dokhan Volcanic Suite, South Safaga Area, Egypt: The Role of Late Neoproterozoic Crustal Extension. *Precambrian Research*, V. 125, pp. 161-178. [http://dx.doi.org/10.1016/S0301-9268\(03\)00110-4](http://dx.doi.org/10.1016/S0301-9268(03)00110-4)
- [37] Mor, D. and Steinitz, G., 1985: The history of the Yarmouk River based on K-Ar dating and its implication on the development of the Jordan rift. *Isr. Geol. Surv. Rep. GSI/40/85*, pp. 18, Jerusalem.
- [38] Norry, M. J. and Fitton, J. G., 1993: Compositional Differences between Oceanic and Continental Basic Lavas and Their Significance. In: Hawkes worth, C. J. and Norry, M. J., Eds., *Continental Basalts and Mantle Xenoliths*, Shiva Publishing Ltd., Cheshire, pp. 5-19
- [39] Pearce, J. A. and Cann, J. R., 1973: Tectonic Setting of Basic Volcanic Rocks Determined Using Trace Element Analyses. *Earth and Planetary Science Letters*, V. 19, pp. 290-300. [http://dx.doi.org/10.1016/0012-821X\(73\)90129-5](http://dx.doi.org/10.1016/0012-821X(73)90129-5)
- [40] Pearce T. H., Gorman, B. E. and Birkett, T. C., 1977: The Relationship between Major Element Chemistry and Tectonic Environment of Basic and Intermediate Volcanic Rocks. *Earth and Planetary Science Letters*, V. 36, pp. 121-132. [http://dx.doi.org/10.1016/0012-821X\(77\)90193-5](http://dx.doi.org/10.1016/0012-821X(77)90193-5).
- [41] Pearce J. A., 1983: Role of the sub-continental lithosphere in magma genesis at active continental margins. In: Hawkes worth C. J. and Norry M. J. (eds), *Continental basalts and mantle xenoliths*. Shiva, Nantwich, pp. 230-249.
- [42] Pearce, J., Harris, N. and Tindle, A., 1984: Trace Element Discrimination Diagram for the Tectonic Interpretation of Granitic Rocks. *Journal of Petrology*, V. 25, pp. 956-983. <http://dx.doi.org/10.1093/petrology/25.4.956>
- [43] Peltz, S. and Bratosia W., 1986: New Data on the Geochemistry of the Quaternary Basalts in Pensani Mountains. *Geophics*, V. 71, pp. 389-403
- [44] Poncarov, V. P., Kazmin, V. G., Mikhailov, L. A., Razvaliyev, A. V., Krashennnikov, A. V., Kozlov, V. V., Souidi-Kondratyev, E. D., Mikhailov, K. YA., Kulakov, V. V., Faradzhev, V. A., Mirzayev, K. M., 1967: The geology of Syria. Explanatory Notes of the geological map of Syria, Part 1. Dept. of Geological and Mineral Research. S. A. R.
- [45] Rollinson, H. R., 1993: Using Geochemical Data: Evaluation, Presentation, Interpretation. Longman Scientific and Technical, England. p. 352.
- [46] Shaw, J. E., Baker, J. A., Menzies, M. A., Thirlwall, M. F. and Ibrahim, K. M., 2003: Petrogenesis of the Largest Intraplate Volcanic Field on the Arabian Plate (Jordan): A Mixed Lithosphere-Asthenosphere Source Activated by Lithospheric Extension. *Journal of Petrology*, V. 44, pp. 1657-1679. <http://dx.doi.org/10.1093/petrology/egg052>
- [47] Shaw, J. (2003): Geochemistry of Cenozoic Volcanism and Arabian Lithospheric Mantle in Jordan. Unpublished PhD. Thesis, University of London, London.
- [48] Smadi Ali K., (2016): Mineralogy, Geochemistry and petrogenesis of selected basaltic outcrops in central parts of Irbid Governorate, North Jordan. Master of Science in Geology Thesis, Yarmouk University, Irbid Jordan, pp.137.
- [49] Steinitz, G. and Baratov, Y., 1992: The Miocene-Pleistocene history of the Dead Sea Segment of the Rift in Light of K-Ar Age of Basalts. *Israel Journal of Earth Sciences*, V. 40, pp. 199-208.
- [50] Sun, S. S. and Mac Donough, W. F., 1989: Chemical and Isotopic Systematic of Oceanic Basalts Implications for Mantle Composition and Processes in Magmatism in the Ocean Basins. Geological Society, London, Special Publication, V. 42, pp. 313-345. <http://dx.doi.org/10.1144/GSL.SP.1989.042.01.19>
- [51] Tarawneh K, S. Ilani, I. Rabba, Y. Harlavan, S. Peltz, K. Ibrahim, R. Weinberger and G. Steinitz, 2000: Dating of the Harat Ash Shaam Basalt Northeast Jordan. Report GSI/2/2000: Jordan, Natural Resources Authority (NRA), and Geological Survey of Israel, Jerusalem.
- [52] Thompson, R. N., 1987: Phase Equilibria Constraints on the Genesis and Magmatic Evolution of Oceanic Basalts. *Earth Science Reviews*, V. 24, pp. 161-210. [http://dx.doi.org/10.1016/0012-8252\(87\)90023-7](http://dx.doi.org/10.1016/0012-8252(87)90023-7)
- [53] Wilson, M., 1989: *Igneous Petrogenesis*. Unwin Hyman Ltd., London, pp. 466. <http://dx.doi.org/10.1007/978-1-4020-6788-4>.
- [54] Winter, J. D. 2001: An Introduction to Igneous and Metamorphic Petrology. Prentice Hall Inc., Upper Saddle River, pp. 697.
- [55] Wiesemann, G., Abdullatif, A., 1963: Geology of The Yarmouk Area, North Jordan. Unpubl. Rept. With 10 Petrography, Geochemistry, and Tectonic Setting, North Jordan geol. maps, scale 1:10,000. Fed. Inst. of Geosc. and Nat. Res., Hannover; nat. res. auth., Amman.